JTTEE5 19:541–550
DOI: 10.1007/s11666-009-9458-3
1059-9630/$19.00 © ASM International

Cr_3C_2-NiCr HVOF-Sprayed Coatings: Microstructure and Properties Versus Powder Characteristics and Process Parameters

Maria Prudenziati, Gian Carlo Gazzadi, Marcello Medici, Gregorio Dalbagni, and Marco Caliari

(Submitted February 18, 2009; in revised form September 24, 2009)

Two 75%Cr_3C_2-25%NiCr feedstock powders with the same size distribution but different production process were characterized and found quite different in terms of morphology and phase composition. The powders were sprayed in a HVOF Diamond Jet (Sulzer Metco DJ-2600) torch with five different values of the oxygen-to-hydrogen ratio in order to assess the influence of this parameter on the microstructure and properties of the coatings. The results show that the closed and dense microstructure of one powder (Woka 7302) results in coatings with lower amount of decarburization, less oxide formation and higher toughness compared to coatings from the other powder (Praxair 1375). It was found that the O_2/H_2 ratio impacts mainly on the Young's modulus, which almost doubled by changing the ratio from 0.40 to 0.50, and on toughness, but does not notably affect the Vickers hardness.

Keywords carbon loss, hardness, microstructure of powders and coatings, oxidation, phase composition of powders and coatings, toughness, Young's modulus

1. Introduction

Thermal sprayed carbide coatings, both WC-Co and Cr_3C_2-NiCr cermets, are extensively used for wear- and corrosion-resistant applications (Ref 1-10). Coatings of the WC-Co system generally have a high hardness and wear resistance (Ref 8, 11). However, the decarburization of WC, primarily into W_2C, leads to degradation of properties and limits the application of the coatings to temperatures in the range of 500 °C (Ref 5). On the other hand, Cr_3C_2-NiCr can be used in corrosive environment at service temperatures up to 800 °C; its hardness decreases by increasing the temperature above 600 °C but exhibits good erosion resistance up to 800 °C (Ref 12). Hence, Cr_3C_2-NiCr coatings are ideally suited as protective layers in corrosive environment at elevated temperatures (Ref 7); coatings on steam turbine blades and boiler tubes against erosive wear and corrosion attack are just only a few examples of applications relying on these properties (Ref 11-13).

Extensive research on these carbide cermets has contributed to processing and microstructure characterization as well as to the evaluation of corrosion resistance, mechanical and tribological properties, including effects of oxidation, decarburization and phase transitions. Correlations were reported between coating properties and fuel type (Ref 2), thermal spray method as for example detonation-gun (D-gun), HVOF, HVAS and air plasma spray (APS) (e.g. Ref 9, 14, 15), powder preparation procedure (e.g. Ref 5, 8, 11, 16). Nevertheless, some topics, for example, the various steps of decarburization and deposition efficiency, or evaporation versus rebound effect, are still controversial (Ref 14, 16).

This is not surprising because of the complexity of these cermets, and the myriad of variables involved in their deposition. However, conflicting descriptions and contentions among various authors may result from the restricted information on powders/coatings morphology and microstructure provided by the limited analytical methods used.

The aim of this work is twofold. On one side we intend to approach the characterization of powders and coatings with high-resolution FIB-SEM imaging, together with other more commonly used spectroscopies and ancillary analytical techniques; on the other side we aim at assessing the degree of sensitivity of two types of Cr_3C_2-NiCr feedstock powders to the oxy-fuel ratio in the HVOF-spraying process. Morphology, phase composition and phase distribution of powders and related coatings were investigated along with carbon loss and oxygen intake, hardness and Young's modulus were measured and toughness was evaluated.

Maria Prudenziati, Department of Physics, University di Modena and Reggio Emilia, Via G. Campi 213/A, I-41100 Modena, Italy; **Gian Carlo Gazzadi**, CNR-INFM S3 National Research Center on nanoStructures and bioSystems at Surfaces, Via Campi 213/A, I-41100 Modena, Italy; and **Marcello Medici, Gregorio Dalbagni,** and **Marco Caliari**, Zocca Officine Meccaniche S.r.l., Via Agucchi 41-45, Funo di Argelato, Bologna, Italy. Contact e-mail: maria.prudenziati@unimore.it.

2. Experimental

2.1 Materials and Sample Preparation

Two types of Cr_3C_2-NiCr feedstock powders were used for this study: one described as ''agglomerated and sintered under hot isostatic pressure'' by Woka 7302, and an ''agglomerated and sintered'' one by Praxair 1375 VM. Both powders have the same nominal composition (75 wt.% Cr_3C_2 and 25 wt.% 80Ni-20Cr alloy) and size distribution ($-45+15$ μm).

Coatings 300-350 μm thick were obtained onto degreased and grit-blasted mild steel coupons (3 × 2 cm), with a HVOF system (Diamond Jet Gun, DJ2600, Sulzer Metco). Samples were sprayed (spray distance of 250 mm) with four different values of the molar oxygen/fuel ratio. This latter includes the stoichiometric O_2/H_2 ratio (0.5) as well as two sub-stoichiometric values (0.40 and 0.45), the second one being the most commonly selected by operators of the Diamond Jet Gun in order to remain in a slightly reducing condition. Finally, an over stoichiometric ratio $O_2/H_2 = 0.55$ was included to investigate the effects of an oxidizing atmosphere.

Precision of the mentioned ratios was evaluated to be ±0.02 and mainly ascribed to the accuracy (±3%) of the gas flow meters. Hereafter each sample is denoted with the letter P or W, for evoking the name of the original feedstock powder, and with a number referring to its spray condition, according to Table 1. Ten specimens in each batch were studied. Coatings prepared with a single type of feedstock powder will be denoted as just W-type or P-type samples.

2.2 Experimental Methods

The phase composition of powders and coatings were investigated by x-ray diffraction, with the diffractometer PANalytical (FEI, Eindhoven, The Netherlands) set in the θ-2θ step scan mode (Cu Kα-Ni filter). The spectra were analyzed with X'PERT High Score Plus software (PANalytical) and the incorporated database.

Morphology and microstructure analyses were performed with scanning electron microscopy (SEM) and x-ray fluorescence. Preliminary investigations were carried out on integral powders' particle and polished samples (both surfaces and cross sections) in an SEM (Philips, model XL-40, Eindhoven, The Netherlands) equipped with backscattered-electron detector (BSD-images), energy dispersive x-ray spectrometer (EDS) and image analysis facilities. High-resolution imaging was performed with Dual Beam system (FEI Strata DB235M) combining a focused ion beam column (Ga Liquid Metal Ion Source-LMIS), and an SEM column (Schottky Field Emission electron source), and equipped with an EDAX system for x-ray fluorescence analyses. Here, the powders' particles as well as the coatings were ''cross-sectioned'' by FIB so that the very hard carbide phases in the soft metal matrix could be exposed to clean view for SEM and EDS, without introduction of artifacts or ''dirt'' exposure to the analytical probe. Images were taken from the secondary electrons generated by the primary electron beam (SED images) or by the FIB ions (CDM-E images) (Ref 17). FIB microscopy, which returns images with high topographic sensitivity, Z-contrast, metal/insulator contrast and grain-orientation contrast (from ion-channeling), turned out to be very powerful in distinguishing the metal and carbide phases of the coatings (Ref 18).

Before inspections, analyses and measurements, the surface of the coatings was polished to a roughness of Ra = 0.2-0.5 μm, and then rinsed in acetone and deionized water.

Gas chromatographic methods were used to determine the carbon content in powders and coatings (CS-800, Eltra GmbH, Germany). The oxygen content of a few samples was also measured with a hot gas extraction equipment (EF-400, Leco GmbH, Germany).

The hardness of the coatings was determined on polished plane surfaces using a Vickers indenter (Wolpert Micro Vickers tester mod. 402 MVD, Hylec Controls, Ausburn, Australia) under three different loads of 0.3, 1 and 30 Kgf, for 15 s. On each sample a minimum of 10 indentations was created. The reported data represent the average HV values and their standard deviation for each series of the whole set of indentations. Likewise ten indentations were done on each sample to measure the Young's modulus using a Vickers micro-indenter (CSM Instruments SA, Peseaux, Switzerland) and applying a 3 N (0.306 Kgf) load at rate of 2400 mN/min. The Young's modulus was extracted according to the Oliver-Pharr method (Ref 19). The reported data are the average values and their standard deviation.

The relative indentation toughness was estimated from the Vickers indentions produced under a load of 30 Kgf, in order to achieve well-defined Palmqvist's type cracks. The diagonals of the indentation (a) and cracks (b) formed at the corners of indentations were measured and used to estimate the characteristic crack length ($c = a + b$) and the indentation fracture toughness values K_i. At least ten

Table 1 Specimen designation and spray conditions

Sample code	H_2 flow, slpm	O_2/H_2 flow ratio	Total flow, slpm	Powder feed rate, g/min	Powder carrier gas, N_2, slpm
P2, W2	586 ± 18	0.40 ± 0.02	1108 ± 65	40	20.5
P3, W3	586 ± 18	0.45 ± 0.02	1108 ± 65	40	20.5
P4, W4	586 ± 18	0.50 ± 0.02	1108 ± 65	40	20.5
P5, W5	586 ± 18	0.55 ± 0.02	1108 ± 65	40	20.5

The first character P or W stands for the feedstock powder, the following number refers to the oxygen/fuel ratio

indentations were measured on each sample; the reported values represent the average of the measured ones. According to the nature of the results, the following expression (Ref 20) was used :

$$K = 0.0123 * E^{2/5} * H^{1/10} * (P/b)^{1/2}$$

where E (N/m^2) is the measured Young's modulus, H (N/m^2) the hardness and P the external load applied.

3. Results

3.1 Microstructure and Composition

3.1.1 Powders. The morphological differences between the two feedstock powders are shown in Fig. 1. The vast majority of Woka particles exhibits a spherical shape and compact structure, with the carbide phase consisting in elongated grains (each carbide grain approximately 4-8 μm long and 2-4 μm wide) totally embedded in the metal matrix; the phase distribution results in very dense and compact particles. On the contrary, the Praxair powder is characterized by a porous structure with elongated particles consisting of micron-sized sub-grains (almost spherical or at least equiaxed grains ranging from about 2 to 6 μm in linear dimension) located on the surface of the particles. Figure 2 emphasizes these differences by showing FIB cross-sections of the particles to expose their internal structure. Here, we can appreciate the capability of the Dual Beam instrument to sculpture single powder particles and to expose a clean cross-section, without the introduction of artifacts or ''dirt'' exposure to the analytical probes, despite the material consists of a hard (carbide)-soft (metal matrix) phase combination. The images clearly show that in the Woka powder the metal matrix (bright areas) completely envelopes the carbide grains (darker areas), resulting in a compact, almost uniform structure. On the contrary, the carbide grains in the Praxair powder are only partially surrounded by the metal alloy and, in addition, the internal space of the particle

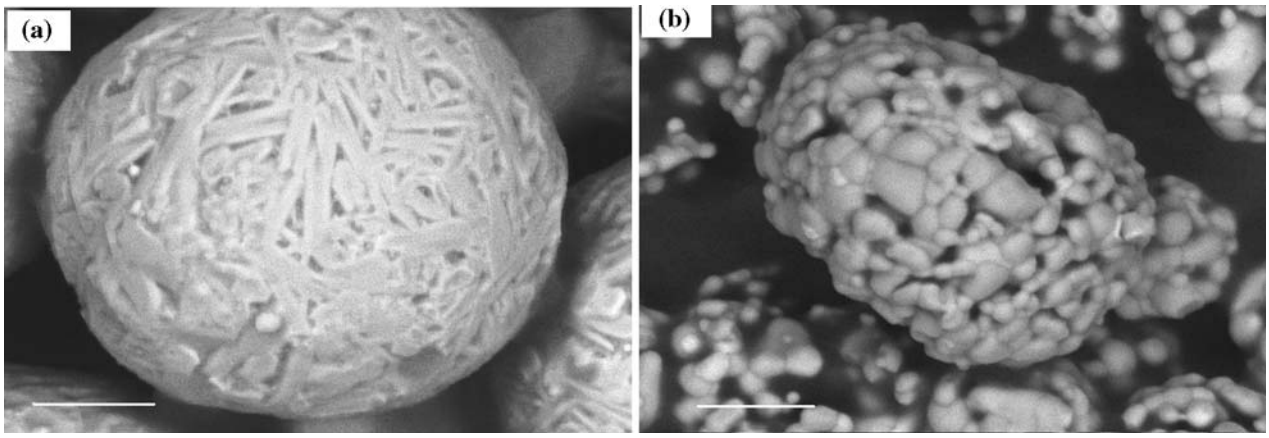

Fig. 1 SEM-BSD images of a particle from the feedstock powders: WOKA 7302 (a) and Praxair 1375 VM (b). Scale marker = 10 μm

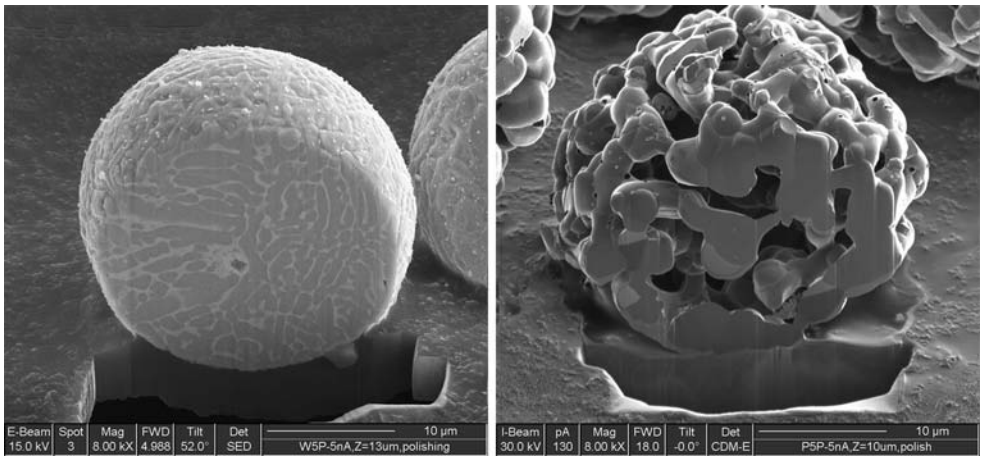

Fig. 2 High-resolution images of FIB-sectioned powder particles: SEM-SED image of WOKA 7302 particle (left) and FIB-CDM image of Praxair 1375 VM particle (right)

leaves large open spaces and ''exposed'' surfaces. The lower mass of the Praxair particles as compared with that of the Woka powder might induce possible rebounding-off effects (Ref 16). We might note some similarity between the morphology of this P-powder and that of ''nano-powders'' (e.g. Ref 21) because of its high porous shell-type morphology, but here the individual grains residing within each particle are much coarser (micron range size diameter) than that of nano-composite particles (sub-micron dia).

Figure 3 presents the x-ray diffraction patterns collected from the two powders. In both cases, we observe very narrow and high peaks, indicating a high level of crystalline order. In both powders, a cubic Ni solid solution is observed (JCPDS 03-065-0380), but Praxair 1375 VM contains a single carbide phase, namely tongbaite (JCPDS 00-035-0804) while Woka 7302 comprises also another polymorph of Cr_3C_2 (JCPDS 03-065-0897); this result likely manifests the different conditions of pressure and temperature used for the powder preparation.

No notable difference in chemical composition between the two powders was detected: only Ni, Cr, and C were detected together with a minor amount of O. Nevertheless, a quantitative evaluation was difficult due to possible addition of O and C during powders' manipulation and to the limited accuracy of an analysis performed on samples too far from the ideal morphology (neither totally dense nor flat).

The content of carbon measured with chromatic analysis is the same within the uncertainty of the measurement, i.e. $9.44 \pm 0.08\%$ by weight and $9.40 \pm 0.06\%$ in Praxair and Woka powders, respectively.

3.1.2 Coatings. Figure 4(a) displays the FIB CDM-E image for sample P2. Here, the high contrast difference between the different regions is due to the sensitivity of FIB imaging to the insulating/conductive nature of materials yielding dark/bright contrast respectively, and also to the different mass densities, affecting the ion penetration range and, as a consequence, the secondary electrons yield. EDS analysis of the region enabled us to recognize the following features in Fig. 4. The very dark isolated regions correspond to Cr_3C_2 grains, while the brighter matrix surrounding them is the Ni-Cr matrix. The higher metallic nature of the Ni-Cr matrix compared to the carbide grains is in agreement with the expected insulating/conductive contrast in FIB imaging; moreover, the carbide is nominally about 20% less dense than the metallic matrix, and this results in deeper ion ranges with lower secondary electrons yield in the surface region.

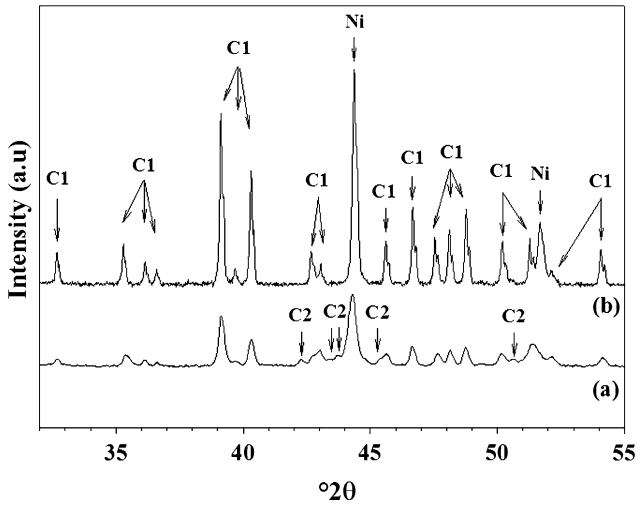

Fig. 3 XRPD patterns of the feedstock powders: (a) Woka 7302 and (b) Praxair 1375 VM. C1: Cr_3C_2 JCPDS 00-035-0804, orthorhombic, space group *Pnam* 62; C2: Cr_3C_2 JCPDS 03-065-0897, orthorhombic, space group *Cmcm* 63. Peaks labeled Ni are due to the Ni solid solution

Carbide grains are quite diversified in size and shapes, mostly with rounded *silhouette*. Various grains (one of them almost in the center of the image) appear fractured in two parts, in such a way to suggest quenching of a fragile material. The matrix around these grains gives rise to a remarkable variety of contrasts. The clearest small regions are rich in Cr and O, in the ratio consistent with the oxide Cr_2O_3. A ''waving'' contrast is noted which suggests the solidification of a low density liquid. The nearly gray background mainly consists of Ni and Cr, but apparently richer in Cr than that in the 80Ni20Cr feedstock powder according to EDS analysis performed in points located between adjacent carbide grains but chosen as far as possible from those grains in order to limit the contribution of Cr pertaining to Cr_3C_2.

This result, as well as the reason of the wide variety of contrast in the image (Fig. 4), demands for further investigations with analytical techniques able to accurately measure the actual composition of points at sub-micrometric distances.

Figure 4(b) shows the SEM-SED image of a FIB cross-section on the same sample P2, enabling an analysis of the coating structure along the vertical direction. We notice that very few small pores are visible; moreover, there is no indication of a structure built up by splat-over-splat, as typically observed in thermally sprayed materials. A ''waving'' contrast is again observed here, similar to that present in the in-plane view.

Figure 5(a) and (b) shows in-plane view and a cross-section in sample P5; these images differ from those collected on the sample sprayed in less oxidizing condition, mainly for the number and extension of fractured carbide grains and amount (volume and number) of oxidized regions.

The in-plane view of sample W2 (Fig. 6a) displays very sharp-edged carbide grains, some of them clearly consisting in fractured parts of the ''parent'' grain, in a nearly uniform background. In addition, the FIB-milled trench (Fig. 6b) reveals the presence of relatively large voids.

In Fig. 7(a) and (b), the morphology of W5 coatings is presented. The in-plane view points out a very dense assemble of carbide grains having less sharp edges than those of grains in W2 sample; they are separated by thin layers of the metal matrix spotted by oxide (the brighter clear regions). The variety of contrast seen in P5 coatings is not so large and evident in these W5 coatings. The FIB trench reveals a large fraction of pores and voids

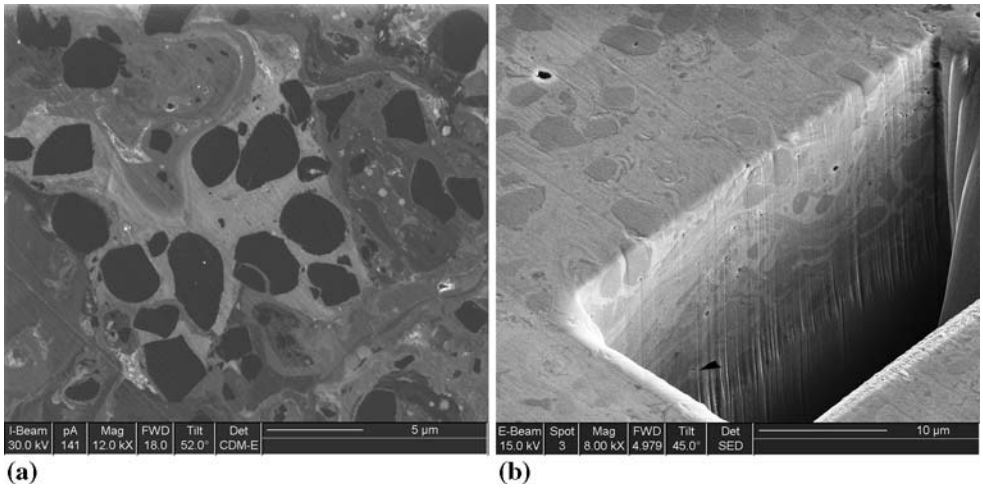

Fig. 4 FIB-CDM-E images of coating P2: (a) in-plane view and (b) exposed wall of a FIB cross-section

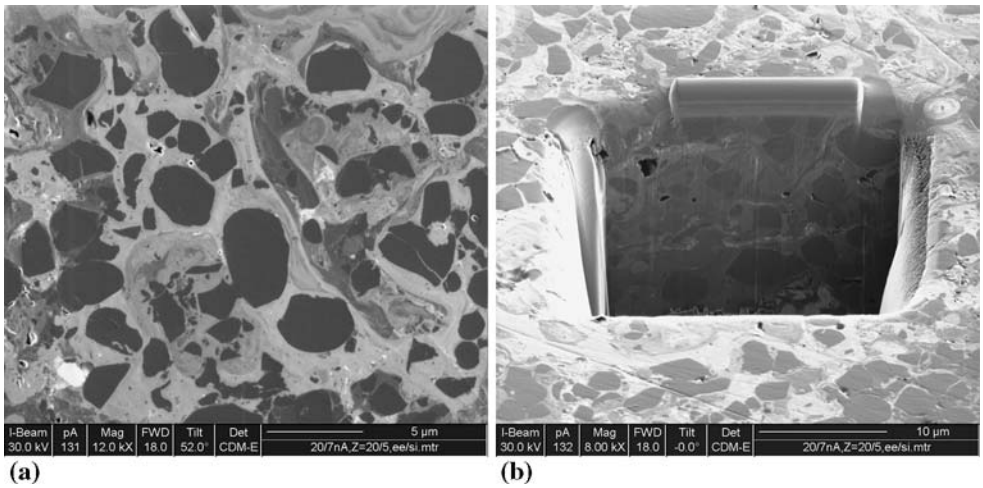

Fig. 5 In-plane view (a) and the exposed wall of a FIB cross-section (b) in the coating P5

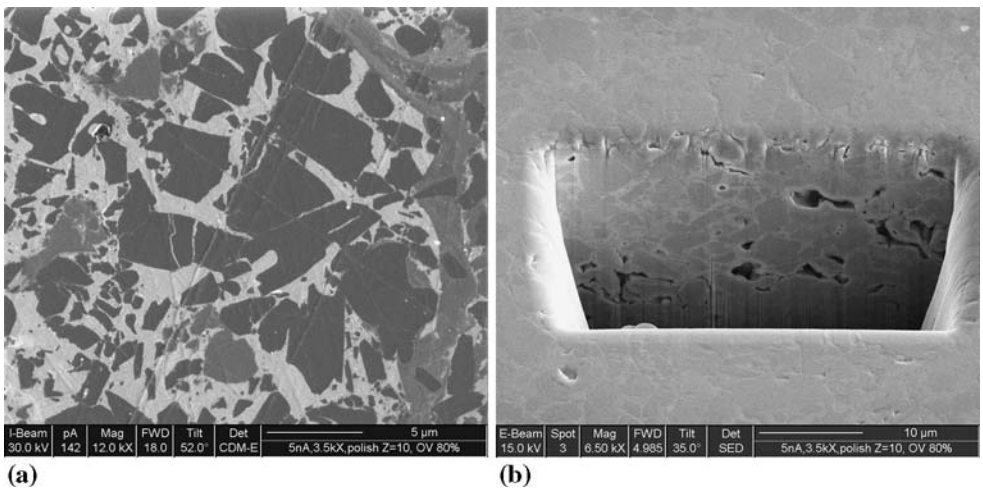

Fig. 6 FIB-CDM-E images of coating W2: (a) in-plane view and (b) exposed wall of a FIB cross-section

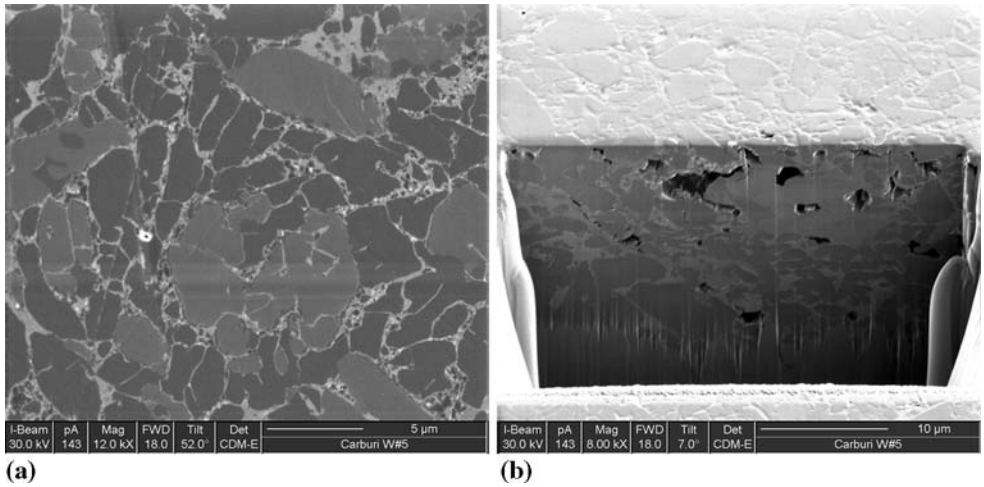

Fig. 7 In-plane view (a) and the exposed wall of a FIB cross-section (b) in the coating W5

embedded in the coatings; also, here no significant evidence of overlapping splats is observable.

Figure 8(a) compares the x-ray diffraction patterns of coatings P2 and P5. Cr_3C_2-tongbaite, NiCr and Cr_2O_3 phases, were detected in all the P-type coatings regardless of the spraying conditions, but the peak heights change with the oxygen/fuel ratio, i.e. larger the latter, lower the apparent amount of NiCr as well as of Cr_3C_2 phases, whereas simultaneously the presence of Cr_2O_3 becomes progressively more evident. All peaks are very broad, notably the one centered around 43°, ascribed to an amorphous or semi-crystalline supersaturated solid solution (Ref 14, 15).

Samples from W2 to W5 give identical XRPD patters (Fig. 8b), i.e. they display the same peaks, at identical angular position and equal intensity, regardless of the O_2/H_2 ratio during the spraying process. The peaks correspond to the same phases identified in P2-P5 samples, i.e. Cr_3C_2-tongbaite, NiCr and Cr_2O_3, but with a minor evidence of Cr_2O_3 peaks. A further notable difference between the XRPD patterns of W-type and P-type samples concerns the background and the area of the peak around 43°, both being lower in W-type samples as compared to P-type samples (e.g. Fig. 8c), indicating a lower amount of amorphous or semi-crystalline phases in W-type coatings.

The results of the carbon analyses are listed in Table 2. Clearly in P-type coatings the carbon content is significantly lower (~20%) than that in the parent powder, without an apparent dependence of the O_2/H_2 ratio; the decarburization in the Woka-type coatings is comparatively insignificant.

3.2 Mechanical Properties

Figure 9 illustrates the way in which the spray process impacts on the Young's modulus of our coatings. A common feature of results for the two types of samples is the increase of the modulus, almost doubling by increasing the O_2/H_2 ratio from sub-stoichiometric to stoichiometric conditions. The subsequent *decrease* of the modulus, especially prominent in W-type samples, is interpreted as a result of the large number of voids in the samples at high oxygen/fuel ratio (Fig. 7) and/or subsiding of ''weak superficial regions'' under the indenter action (Fig. 10). In both cases, the pressure exercised by the indenter is responsible for a partial collapse of the coating and therefore the measurement indicates a false (inferior) resilience of the solid. The larger data scattering for W-type samples compared to the P-type counterparts is probably another indication of the same effect.

SEM images of typical Vickers indentations are shown in Fig. 10. Statistically, more than 50% of tests under 0.3 Kgf resulted in ''clean'' indents, i.e. without cracks (e.g. Fig. 10a) both on the corner or near the sides of the Vickers shapes. Frequent occurrences of cracks (such as those shown in Fig 10b) are visible after tests with indenter load of 1 Kgf, but well developed median cracks of the Palmquist's type appear after 30 kg applied load (Fig. 10c); in the latter case, the indent depth is lower than one-seventh of the coating thickness (≥300 µm), a condition making the contribution of the substrate to the plastic deformation negligible (Ref 22).

Table 3 lists the results of the Vickers hardness tests (average values and their standard deviation) for the various loads, together with the relative indentation toughness.

P-type coatings exhibit the following:

(a) A clear decrease of the measured hardness, by increasing the applied load from 0.30 to 30 Kgf, a finding already reported and explained in terms of inter-lamellar boundaries opening (Ref 10). The concurrent lower scatter of measured data leads to a lower standard deviation than that observed for the load of 0.3 Kgf, the most commonly used one (e.g. Ref 9).
(b) A slight decrease of the hardness (average values) by increasing the O_2/H_2 ratio.
(c) A moderate increase of the toughness by increasing the oxy-fuel ratio.

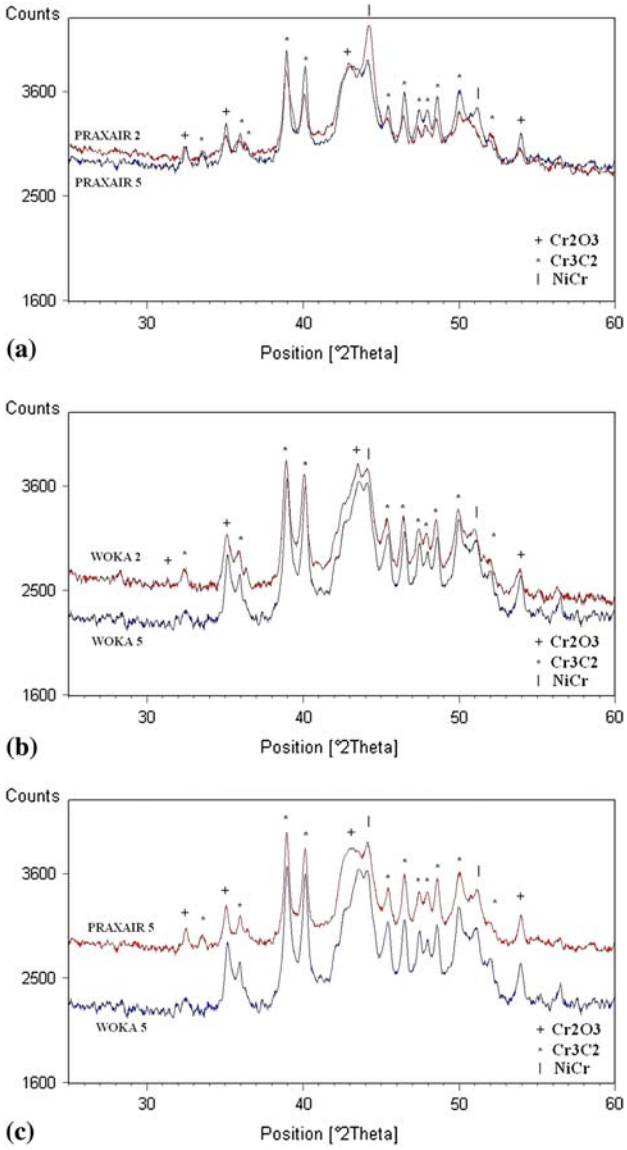

Fig. 8 XRPD patterns of coatings prepared in different spray conditions: (a) P-type coatings sprayed under low (Praxair 2) and high (Praxair 5) oxy-fuel ratios; (b) W-type coatings sprayed under low (Woka 2) and high (Woka 5) oxy-fuel ratios; (c) P-type and W-type coatings sprayed with the same super-stoichiometric oxy-fuel ratio

The difference between measured values for W-type samples is not significantly larger than the uncertainty of the measurements making unfeasible any scheme of correlation between the hardness and toughness on one side and load and O_2/H_2 on the other one. However, a comment on the particularly deviating trend in toughness values (Table 3, coating W5) is mandatory: the sharp decrease in toughness in W5 samples is the result of the decrease in Young's modulus (Fig. 9) that enters in Eq 1. On the other hand, the measurement of Young's modulus, as previously noted, is especially affected by voids and lack in cohesion between splats in W5 samples.

Table 2 Carbon and oxygen content in feedstock powders and coatings

Sample	Carbon, wt.%	Oxygen, wt.%
Praxair powder	9.44 ± 0.08	…
P2	7.64 ± 0.06	3.1 ± 0.3
P3	7.39 ± 0.22	
P4	7.53 ± 0.45	
P5	7.37 ± 0.01	3.7 ± 0.6
WOKA powder	9.40 ± 0.10	…
W2	8.80 ± 0.09	
W3	8.99 ± 0.05	
W4	9.08 ± 0.03	
W5	9.00 ± 0.09	

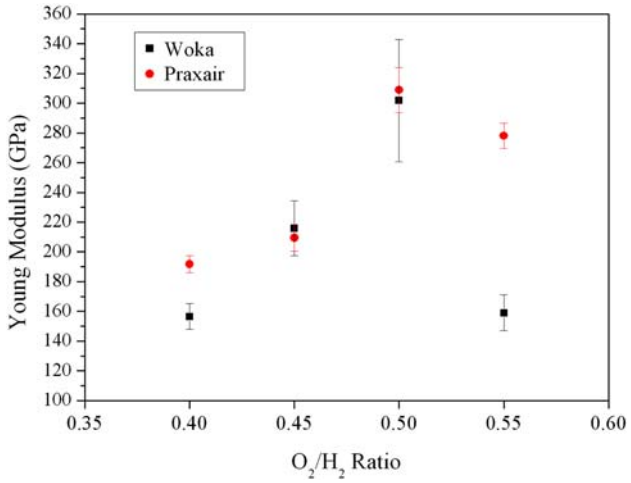

Fig. 9 Measured Young's modulus of P-type and W-type coatings sprayed in different oxygen/fuel conditions

Our results concerning elastic modulus and toughness of coatings prepared at oxy-fuel ratio of 0.45 are comparable with those reported by Roy et al. (Ref 20).

4. Discussion

We have found that powders sintered under hot isostatic pressure consist of particles in which carbide grains are completely embedded in a metal matrix, whereas powders merely sintered are lower in density and compactness. This difference in morphology could be sufficient to interpret the difference in microstructure development of the corresponding coatings. In fact, the metal cladding minimizes the decarburization, whereas the effective surface area offered by porous particles results in a larger carbon loss (Table 2) and oxidation (Fig. 8). In addition, however, these results are consistent with a lower temperature attained by the very dense and compact particles with respect to the looser particles. A less heat-up in the former case is also suggested by the morphological features of the W-type coatings, i.e. shape and cracking of carbide grains as well as minor contrast in

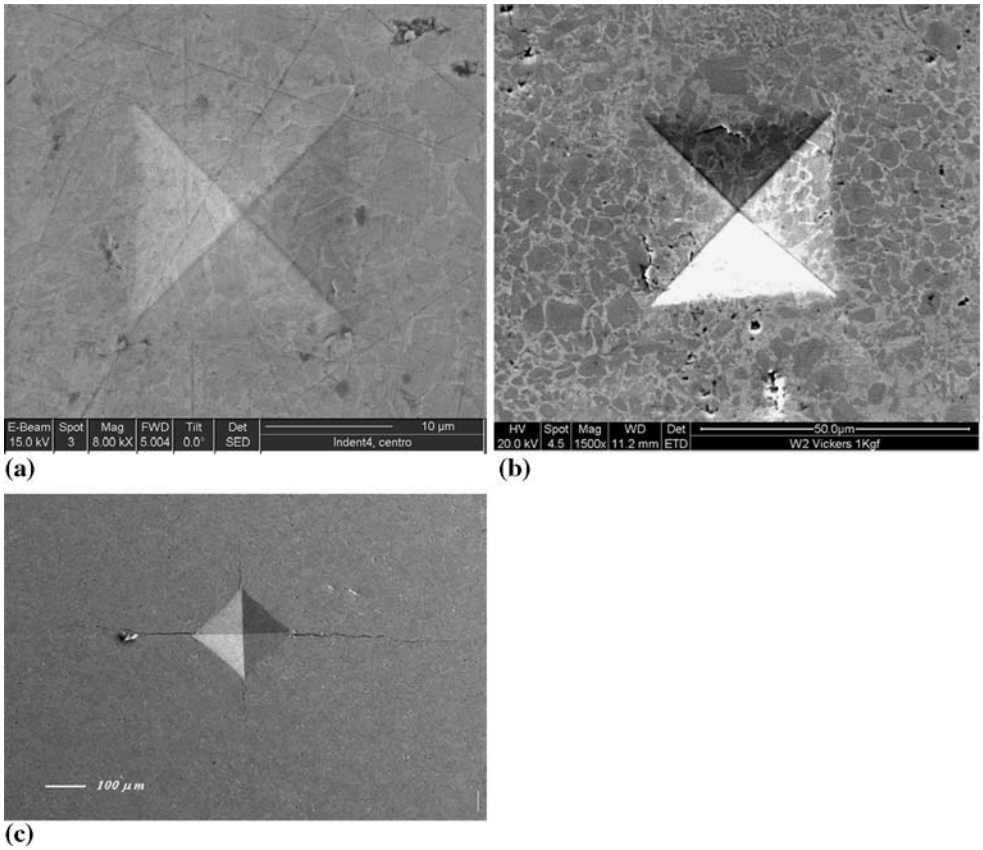

Fig. 10 SEM micrographs showing typical aspects of Vickers indentations: (a) a ''clean'' indent, load of 0.3 Kgf, (b) cracks after a test at a load of 1 Kgf, and (c) Vickers indentation with well-defined Palmquist crack

Table 3 Vickers hardness and indentation toughness of coatings prepared under various oxygen/fuel ratio

Sample	$VH_{0.3kg}$	VH_{1kg}	VH_{30kg}	K_c, MPa√m
P2	1152 ± 103	1128 ± 36	907 ± 50	7.91
P3	980 ± 92	1064 ± 22	836 ± 80	9.43
P4	924 ± 72	956 ± 32	798 ± 12	13.74
P5	857 ± 75	950 ± 30	802 ± 40	11.29
W2	882 ± 178	718 ± 88	725 ± 10	9.26
W3	992 ± 164	777 ± 102	744 ± 13	18.99
W4	843 ± 124	830 ± 123	764 ± 30	37.33
W5	827 ± 140	882 ± 71	798 ± 10	24.06

micrographs of the metal matrix (possibly related to interactions between the coatings' constituents).

Both spraying process (oxygen/fuel ratio) and morphology of the parent powder affect the hardness of the coatings, but not in a simple manner. For example, the higher amount of decarburization of P-type samples (lower content of the hard phase) might suggest a lower hardness of these coatings in comparison with that of W-type samples; this expectation is disproved by the results. One could argue that oxidation plays the major role (P-type samples more oxidized than W-type samples); however, in this case one should observe a decrease in hardness in P-samples by increasing the O_2/H_2 ratio. However, experimental findings show the opposite result. It remains to be explored if other features not fully evaluated yet (e.g. amorphous phases, actual composition of the NiCr matrix or micro-phases) affect the microstructure and then the hardness of these samples.

We measured comparable values of Young's modulus in the two series of samples, despite their different amount of decarburization and oxidation (Table 2 and Fig. 9). In addition, we noted a significant increase of the modulus by changing the oxy-fuel ratio from 0.4 to 0.5, although the overall composition (including the carbon content) does not notably change as a function of the O_2/H_2 ratio. Further studies are needed to understand also these findings.

The seemingly lower elastic modulus measured in coatings prepared in over-stoichiometric conditions (i.e. $O_2/H_2 = 0.55$), and especially evident in W-type samples, correlates with the presence of cavities (large pores) or subsiding material under the indented surface.

It is appropriate to stress here that the widespread method for evaluation of decarburization in WC-Co spray coatings, i.e. the analysis of diffraction peaks (Ref 23), is not applicable to Cr_3C_2-NiCr coatings because of the strong similarity between the peaks of the different chromium carbide phases. Elemental analyses are therefore more important for measuring the carbon content in chromium carbides coatings, whereas techniques with very

high spatial resolution need to be applied for better information of the phase distribution in the coatings.

Finally, the results of this study demonstrate the utility of FIB imaging in the advanced characterization of feedstock powders and thermally sprayed coatings, to supply detailed information in their microstructure and to provide insights in the spraying processes. FIB cross-sectioning of coatings effectively preserves their microstructure, without time-consuming procedures such as precision cutting, infiltration with resins and polishing and without the need of optimizing the metallographic preparation in order to avoid sample damage. Examples of recognized potentially harmful effects for a correct inspection of the microstructure are the localized material removal (pulls out) during cutting, grinding and polishing stages and smearing of material over the voids, mainly during cutting and planar polishing stages (Ref 24). These effects might be particularly severe in cermets comprised of very hard grains in a relatively soft matrix, such as Cr_3C_2-NiCr coatings. Polishing-induced pull outs of plasma sprayed Cr_3C_2-NiCr coatings were in fact observed by Li and Ding (Ref 25).

5. Conclusions

Two Cr_3C_2-NiCr feedstock powders, one ''agglomerated and sintered under hot isostatic pressure'' (W powders) and the other one ''agglomerated and sintered'' (P powders), were found to exhibit a very different microstructure: carbide grains are completely embedded in the metal matrix of W powders, whereas particles of the P powders exhibit an ''open'' structure, lower density and compactness. These differences result in significant lower amounts of decarburization ($<10\%$) and lower oxidation in W-type sprayed coatings than in P-type coatings, in which the carbon loss is about 20%. Microstructural characterization suggests enhanced interactions between carbide grains and the metal matrix due to a higher temperature attained by P powders than that reached by the W powders. These results are essentially independent of the oxidative conditions set during the HVOF spray process, i.e. the oxy-fuel ratio O_2/H_2 varied from 0.4 to 0.55.

On the contrary, the oxy-fuel ratio appears to affect, in a complex way, some features of microstructure and mechanical properties of the coatings.

A synthesis of the results is as follows:

A series of Vickers hardness measurements (1 Kgf load) shows a decrease of the hardness for P-type samples as a function of the O_2/H_2 ratio; the opposite trend (decrease in HV vs. O_2/H_2 ratio) is observed for the W-type samples. Measurements under lower (0.3 Kgf) and higher (30 Kgf) loads systematically give too scattered values, especially for W samples, to confirm these interesting trends.

Despite the large standard deviations of data, it is possible to state that for coatings sprayed under sub-stoichiometric conditions ($O_2/H_2 < 0.5$) P-type samples exhibit higher hardness and relatively lower toughness than W samples.

Comparable values of the Young's modulus are measured in the two series of samples and a monotonous increase observed as a function of the oxy-fuel ratio till $O_2/H_2 = 0.5$, but a sudden drop at $O_2/H_2 = 0.55$.

A critical analysis of these complex behaviors suggests the need of further analyses to explore the possibility that interactions between the carbide grains and the metal matrix are responsible for changes in microstructure which in turn notably impact on the mechanical properties of Cr_3C_2-NiCr HVOF-sprayed coatings.

Acknowledgments

The authors thank the Surface Engineering and Ceramic Unit (Ing. Roberta Valle) of Centro Sviluppo Materiali S.p.A, Rome, for assistance in Vickers indentations at high load. Also, the collaboration of Colleagues of the Program Net-Lab ''Surface and Coatings for Advanced Mechanics and Nanomechanics'' (SUP&RMAN) supported by Regione Emilia e Romagna is acknowledged.

References

1. M. Mohanty, R.W. Smith, M. De Bonte, L.P. Celis, and E. Lugscheider, Sliding Wear Behaviour of Thermally Sprayed 75/25 Cr_3C_2/NiCr Wear Resistant Coatings, *Wear*, 1996, **198**(1-2), p 251-266
2. S. Zimmermann and H. Kreye, Chromium Carbide Coatings Produced with Various HVOF Spray Systems, *Thermal Spray: Practical Solutions for Engineering Problems, Proceedings of the National Thermal Spray Conference, 9th*, C.C. Berndt, Ed., October 7-11, 1996 (Cincinnati), ASM International, Materials Park, OH, p 147-152
3. H.L. de Villiers Lovelock, Powder/Processing/Structure Relationships in WC-Co Thermal Spray Coatings: A Review of the Published Literature, *J. Therm. Spray Technol.*, 1998, **7**(3), p 357-373
4. R. Schwetzke and H. Kreye, Microstructure and Properties of Tungsten Carbide Coatings Sprayed with Various High-Velocity Oxygen Fuel Spray Systems, *J. Therm. Spray Technol.*, 1999, **8**(3), p 433-439
5. G. Matthäus, J.A. Picas, and A. Forn, Effect of Feedstock Powder Size on the Sliding Wear Behavior of Thermal Sprayed HVOF Cr3C2-NiCr Coatings, *Thermal Spray 2004: Advances in Technology and Application, Proceedings of the International Thermal Spray Conference*, Osaka, Japan, May 10-12, 2004, p 32-36
6. l.-M. Berger, M. Woydl, S. Zimmerman, H. Keller, G. Schwier, R. Enžl, and S. Thiele, Tribological Behavior of HVOF-Sprayed Cr_3C_2-NiCr and TiC-Based Coatings Under High-Temperature Dry Sliding Conditions, *Thermal Spray 2004: Advances in Technology and Application, Proceedings of the International Thermal Spray Conference*, Osaka, Japan, May 10-12, 2004, p 5-14
7. B.Q. Wang, A Comparison of Elevated Temperature Erosion Resistance of Several Carbide Cermet Coatings, *Tagungsband Conference Proceedings*, E. Lugscheider, Ed., DVS-Deutscher Verband für Schweißen, Germany, 2002, p 926-929
8. A. Kirsten, M. Oechsle, and R.F. Moll, Carbide Containing Materials for Hard Chromium Replacement by HVOF-Spraying, *International Thermal Spray Conference Basil, Thermal Spray Connects: Explore its Surfacing Potential!* E. Lugscheider, Ed., Switzerland May 2-4, 2005, DVS-Verlag GmbH, Duesseldorf, Germany, 2005, p 957-962
9. G. Barbezat, A.R. Nicol, and A. Sickinger, Abrasion, Erosion and Scuffing Resistance of Carbide and Oxide Ceramic Thermal Sprayed Coatings for Different Applications, *Wear*, 1993, **162-164**(Part 1), p 529-537

10. J.F. Li, X.Y. Wang, H. Liao, C.X. Ding, and C. Coddet, Indentation Analysis of Plasma-Sprayed Cr_3C_2-NiCr Coatings, *J. Mater. Sci.*, 2004, **39**(23), p 7111-7114
11. I. Fagoaga, J.L. Viviente, P. Gavin, J.M. Bronte, J. Garcia, and J.A. Tagle, Multilayer Coatings by Continuous Detonation System Spray Technique, *Thin Solid Films*, 1998, **317**(1,2), p 259-265
12. G.-J. Yang, C.-J. Li, S.-J. Zhang, and C.-X. Li, High-Temperature Erosion of HVOF Sprayed Cr_3C_2-NiCr Coating and Mild Steel for Boiler Tubes, *J. Therm. Spray Technol.*, 2008, **17**(5-6), p 782-787
13. B.Q. Wang, Effect of Alkali Chlorides on Erosion-Corrosion of Cooled Mild Steel and Cr_3C_2-NiCr Coating, *Wear*, 1996, **199**(2), p 268-274
14. S. Matthews, M. Hyland, and B. James, Microhardness Variation in Relation to Carbide Development in Heat Treated Cr_3C_2–NiCr Thermal Spray Coatings, *Acta Mater.*, 2003, **51**(14), p 4267-4277
15. F. Otsubo, H. Era, T. Uchida, and K. Kishitake, Properties of Cr_3C_2-NiCr Cermet Coating Sprayed by High Power Plasma and High Velocity Oxy-Fuel Processes, *J. Therm. Spray Technol.*, 2000, **9**(4), p 499-504
16. C.-J. Li, G.-C. Ji, Y.-Y. Wang, and K. Sonoya, Dominant Effect of Carbide Rebounding on the Carbon Loss During High Velocity Oxy-Fuel Spraying of Cr_3C_2–NiCr, *Thin Solid Films*, 2002, **419**(1-2), p 137-143
17. F.A. Stevie, L.A. Giannuzzi, and B.I. Prenitzer, The Focused Ion Beam Instrument, *Introduction to Focused Ion Beams—Instrumentation, Theory, Techniques and Practice*, L.A. Giannuzzi and F.A. Stevie, Ed., Springer, New York, 2005, p 1-12
18. T. Suzuki, N. Endo, M. Shibata, S. Kamasak I, and T. Ichinokawa, Contrast Differences Between Scanning Ion and Scanning Electron Microscope Images, *J. Vac. Sci. Technol. A*, 2004, **22**(1), p 49-52
19. W.C. Oliver and G.M. Pharr, Measurement of Hardness and Elastic Modulus by Instrumented Indentation: Advances in Understanding and Refinements to Methodology, *J. Mater. Res.*, 2004, **19**(1), p 3-20
20. M. Roy, A. Pauschitz, J. Bernardi, T. Koch, and F. Franek, Microstructure and Mechanical Properties of HVOF Sprayed Nanocrystalline Cr3C2-25(Ni20Cr) Coating, *J. Therm. Spray Technol.*, 2006, **15**(3), p 372-381
21. B.H. Kear, R.K. Sadangi, M. Jain, R. Yao, Z. Kalman, G. Skandan, and W.E. Mayo, Thermal Sprayed Nanostructured WC/Co Hardcoatings, *J. Therm. Spray Technol.*, 2000, **9**(3), p 399-406
22. A. Tricoteaux, E.S. Puchi-Cabrera, and L. Lesage, Method for Fast Determination of Thin Films Hardness from Standard Microindentation Tests, *Surf. Eng.*, 2007, **23**(1), p 40-44
23. B.H. Kear, G. Skandan, and R.K. Sadangi, Factors Controlling Decarburization in HVOF Sprayed Nano-WC/Co Hard Coatings, *Scr. Mater.*, 2001, **44**(8/9), p 1703-1707
24. E. Kharlanova and I. Grigore, Optimization of Metallographic Preparation for Thermally Sprayed Coatings Using Taguchi-Method, *Proceedings of the International Thermal Spray Conference "Tagungsband Conference Proceedings"*, E. Lugscheider, Ed., DVS, Deutscher Verband für Schweißen, Essen, Germany, 2002, p 397-3911
25. J.F. Li and C.X. Ding, Polishing-Induced Pull Outs of Plasma Sprayed Cr_3C_2-NiCr Coating, *J. Mater. Sci. Lett.*, 1999, **18**(21), p 1719-1721